Measurements of H_β Stark central asymmetry and its analysis through standard theory and computer simulations

S. Djurović,[1] M. Ćirišan,[1] A. V. Demura,[2] G. V. Demchenko,[2] D. Nikolić,[3] M. A. Gigosos,[4] and M. Á. González[5]
[1]*Department of Physics, Faculty of Sciences, Trg Dositeja Obradovića 4, 21000 Novi Sad, Serbia*
[2]*HEPTI, RRC "Kurchatov Institute," Kurchatov Square 1, Moscow 123182, Russia*
[3]*Department of Physics, Western Michigan University, Kalamazoo, Michigan 49008, USA*
[4]*Departamento de Óptica, Universidad de Valladolid, 47071 Valladolid, Spain*
[5]*Departamento de Física Aplicada, Universidad de Valladolid, 47071 Valladolid, Spain*
(Received 9 November 2007; revised manuscript received 19 December 2008; published 9 April 2009)

Experimental measurements of the center of the H_β Stark profile on three different installations have been done to study its asymmetry in wide ranges of electron density, temperature, and plasma conditions. Theoretical calculations for the analysis of experimental results have been performed using the standard theory and computer simulations and included separately quadrupolar and quadratic Stark effects. Earlier experimental results and theoretical calculations of other authors have been reviewed as well. The experimental results are well reproduced by the calculations at high and moderate densities.

DOI: 10.1103/PhysRevE.79.046402 PACS number(s): 52.70.−m, 32.70.Jz, 52.65.Yy, 32.70.−n

I. INTRODUCTION

Stark-broadened hydrogen lines are a powerful tool in plasma diagnostics (see, for example, Chap. 10 in [1] and references therein). In many cases, electron density is determined with sufficient accuracy from the full width at half-maximum (FWHM) of a measured line. In particular, the H_β line is one of the most deployed lines, and its use has become a standard technique in plasma spectroscopy. This is mainly due to the fact that it is a well isolated line at low and moderate electron densities with a FWHM that is strongly dependant on the electron density and at the same time practically insensitive to changes in plasma electron temperature. Furthermore, the quantity and quality of the available experimental data on this spectral line provide an excellent test case for theoretical models and computational methods [2–10].

No theoretical model can advance if it does not give good results for the H_β line. This happened, for example, when the experiments clearly proved the dependence of the H_β dip on the emitter-perturber reduced mass [4,6,11–13], which at the time gave rise to calculations of line profiles incorporating ion dynamics [14–19]. However, persistent discrepancies between experimental measurements and theoretical calculations have been a hallmark of dense low-temperature plasmas since the very first experimental observations of this line. The experimental profiles showed an asymmetry while some of the most commonly used theoretical models, due to the employed approximations, gave unshifted symmetrical profiles [20–22]. The causes of the H_β line shift and asymmetry, though analyzed many times both theoretically [23–33] and experimentally [9–11,13,34–44], are not clearly quantified.

To our knowledge, the first attempt to explain the H_β line asymmetry relied on the quadratic Stark effect (QSE) in the static ion microfield [45] (for review, see [30,46] and references therein). Later on, the ion-atom quadrupole interaction (QI) [23] was identified and analyzed as the source of asymmetry. The ever increasing experimental accuracy revealed difficulties in the attempts to explain the observed H_β Stark profile asymmetry using only the notion of ion-atom quadrupole interaction [33] with partial account of the static quadratic Stark effect [31,47–49]. More recently, the sources of line asymmetry were analyzed in terms of plasma coupling and microfield dynamical effects as well (see, for example, [29,30,50–52]). The comparison of the values of several H_β asymmetry characteristics, obtained with recent theoretical developments and with respect to changes of the reference point in the wavelength scale, have revealed noticeable remaining discrepancies between experiment and calculations [33,44].

The existing discrepancies hindered the use of this line as a diagnostic tool for high-density plasma conditions. Indeed, it is much more reliable to obtain the plasma electron density by fitting the full theoretical and experimental profiles [1] instead of only using the line FWHM. However, discrepancies between theory and experiment due to the line asymmetry and shift, as well as microfield dynamics and related kinetic effects, tampered the theory-experiment fitting and, in many cases, forced one to do it without considering the central part of the profile when doing the necessary comparisons [53].

Thus the idea of this work is to undertake joint experimental and theoretical benchmark studies of the central part of H_β to study the sources of asymmetry of the Stark profiles, which would improve the possibilities of plasma diagnostics. The fundamental problem studied here is the influence of ion and electron joint dynamics on Stark profiles asymmetry.

We report on experimental measurements conducted in three different settings in order to obtain data in a wide range of electron densities and temperatures. The measured experimental results are compared with existing experimental data [9,12,13,36,38,40–42], and interpreted in light of earlier and recent theoretical calculations [23,25,30,33,50,51,54–56]. We analyze and discuss different causes of line asymmetry, such as quadrupole effects, quenching collisions, elastic collisions, etc.

According with the fundamental aim of the present work, two different but complementary to each other theoretical approaches have been implemented in this study.

First, we use analytical results derived in the framework of the standard theory (ST), which consistently account for the electronic collision shifts, the quadrupole interaction, and the quadratic Stark effect in the static ion microfield. The main benefit of this approach is a straightforward and systematic inclusion of various effects, which in turn enables us to quantify their importance in overall asymmetry of the H_β Stark profiles. The results of two sets of ST calculations are presented with and without use of the perturbation expansion in the contour over quadrupole interaction.

Secondly, settings of computer simulations are presented that consider jointly the ionic and electronic broadenings on the same footing, so that ion and electron dynamics effects are naturally included. Furthermore, the account of transitions between states with different principal quantum numbers permits us to consider the quadratic Stark effect. In this dynamic approach, the quadrupolar effects have not been taken into account. Both theoretical calculations presented in this work contain the trivial asymmetry contribution due to conversion from the frequency scale to the wavelength scale.

This work is another step toward understanding and accurately reproducing the line asymmetries due to the joint analysis based on extended experimental results for a much wider range of plasma parameters and on recent progress in analytical theory and computer simulations.

II. EXPERIMENT

A. Experimental setup

We continue with the description of three different experimental setups used in this work. In the first setup, the plasma source was an electromagnetically driven T-tube, where one segment was the 27-mm-diam tube supplied with a reflector. The T-tube was energized using a 4 μF capacitor bank charged up to 20 kV. The filling gas was hydrogen at a pressure of 300 Pa. Spectroscopic observations of plasma were made by a 1-m monochromator. The observation point was fixed at 4 mm in front of the reflector. Photomultiplier signals were recorded by an oscilloscope. H_β profiles were scanned at close intervals over the spectral range of ± 30 nm from the line center using a shot-to-shot technique with successive discharges. The details on this experiment are given in Ref. [44].

For the second experiment, the plasma source was a pulsed arc, where the discharge was produced by a capacitor bank of 20 μF, charged up to 9 kV. The discharge pyrex lamp, 15 cm long and 3 cm in diameter, was filled with pure hydrogen at a pressure of 600 Pa. The details of this experiment can be found in Ref. [35].

In the third setup, the plasma source was a wall-stabilized electric arc operating in argon at atmospheric pressure. About 2% of hydrogen was added in the central part of the arc. The current of 30 A was delivered to the arc by a current-stabilized power supply. The details on this experimental setup are presented in Refs. [57,58].

B. Plasma diagnostics

The electron densities measured in T-tube plasma, ranging from 9.6×10^{22} to 8.9×10^{22} m^{-3}, were inferred from the Stark widths of the H_β line profiles. The estimated uncertainties of the electron densities do not exceed $\pm 9\%$. The electron temperatures, ranging from 17 000 to 45 000 K, were determined from line-to-line continuum ratios for the H_β line [59]. The uncertainties for electron temperature measurements are between $\pm 8\%$ and $\pm 15\%$ from the lower to the higher values.

The electron densities measured in pulsed arc plasma, ranging from 1.5×10^{22} to 7.0×10^{22} m^{-3}, were also determined from the Stark widths of the H_β line profiles, with an estimated uncertainty of $\pm 7\%$. A temperature of roughly 10 000 K was determined from the plasma equilibrium relations imposing the local thermodynamic equilibrium and assuming that the precise knowledge of the temperature was not essential for this study.

The electron densities measured in wall-stabilized arc plasma, ranging from 1.6×10^{22} to 3.6×10^{22} m^{-3}, were determined from the measured Stark widths of the H_β lines, while electron temperatures, ranging between 10 000 and 11 000 K, were determined from the Saha-Eggert equation [60].

In most cases, independent plasma diagnostics is required to obtain plasma parameters. However, in the bulk of the measurements reported here, the plasma was formed in pure hydrogen. So there were no other well-studied Stark-broadened lines apart from the H_β that could be used for diagnostic purposes. Besides, in the present experimental setup the interferometric methods were not precise enough because of the very short optical path of a laser beam in plasma (about 27 mm).

Thus the same experimental H_β profiles had to be used for diagnostics and for comparison with the theoretical predictions.

C. H_β profile recording and data processing

In general, the intensity measurements of radiation from pulsed sources, such as electromagnetic shock T-tubes or pulsed arcs, give scattered experimental data due to very short observation times and, to a certain degree, due to plasma irreproducibility. This makes a detailed analysis of the H_β line profile rather difficult, especially the part of the profile maxima. The influence of the scattered data was minimized by averaging each point of the recorded profile from six measurements. At the same time, we devoted great care to preserving all discharge parameters and to monitoring oscilloscope signals for nonstatistical deviations with each shot. The oscilloscope signals, shown in Fig. 1, illustrate the temporal evolution of observed spectral intensity and confirm the discharge reproducibility. In the same figure, upper and lower traces correspond to three oscilloscope recordings at sensitivities of 0.5 and 0.1 V/cm, respectively.

The signal intensities were normalized preliminarily to the spectral sensitivity of the optical system as experimental profiles of the H_β line were rather broad—several tens of nanometers. Further separation of the H_β profiles from the

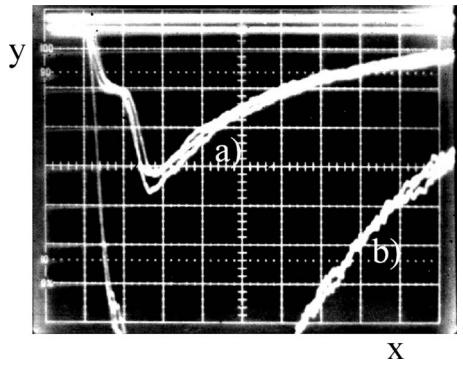

FIG. 1. Relative intensity signals vs the discharge duration time (0.5 ms/cm, x axis) sampled at oscilloscope sensitivities of (a) 0.5 V/cm and (b) 0.1 V/cm (y axis).

contributions of the surrounding H_α and H_γ lines was carried out with the help of Griem's theoretical profiles for these lines [21]. The influence of the H_α line was practically negligible, while the influence of the H_γ line was negligible only in the central part of the H_β profile, but substantial in its blue wing. For example, for the electron densities of $(2-7)\times 10^{23}$ m^{-3}, the H_γ line contribution at detuning from the H_β line center of about two FWHM ranges from 20% to 57%, respectively, while the corresponding contributions at the H_β line center were only 0.3% and 2%. In this analysis, we used plasma temperatures between 19 400 and 34 000 K, respectively, and we also assumed the existence of thermal equilibrium throughout the calculation of the line intensities.

In order to check for nonuniformity and stability, the plasma was monitored by the means of frame and streak photography. As can be judged by the photos in Fig. 2, the plasma image is uniform and does not exhibit any instability pattern due to turbulence.

Before extracting the blue, I_B, and red, I_R, peak intensities, we determine and subtract the continuum level using the asymptotic formula $I=f(\Delta\lambda)^{-5/2}$ [59], which describes the behavior of the spectral intensity in the line wings. The details about the data processing can be found in [44], where possibilities of self-absorption were also discussed.

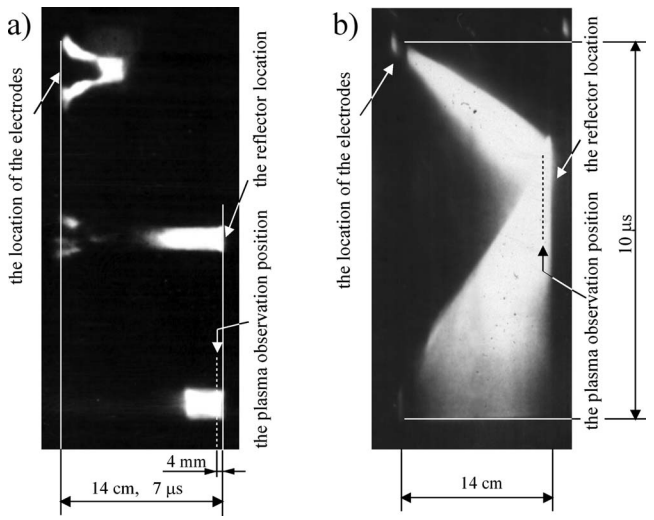

FIG. 2. Frame (a) and streak (b) photography of T-tube discharge.

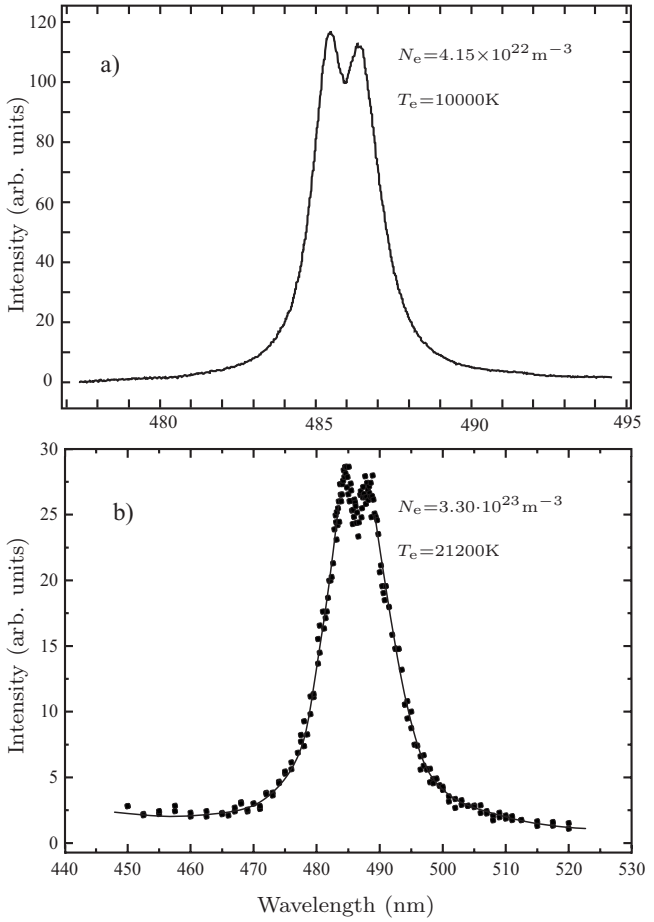

FIG. 3. H_β line profile examples. (a) Pulsed arc experiment, (b) T-tube experiment.

In the second experiment, the spectra were recorded using a spectrometer equipped with an optical multichannel analyzer detector. Each profile was generated from the statistically averaged data of ten discharges. In this experiment, plasma reproducibility was checked comparing all the independently measured discharges for the same conditions and discarding those being obviously wrong due to wrong working of the electric discharge system. Then the final averaged profiles became quite smooth. The self-absorption was measured with the help of a mirror and a lens, imaging the center of the discharge lamp on itself, and was found to be negligible. More details about data processing can be found in Ref. [35].

The third experimental setup used a continuous plasma source, where the spectral line shapes were registered by a strip chart recorder. The self-absorption was checked using a spherical mirror placed behind the arc, and as in two previous setups, was found to be negligible. Two typical examples of experimentally recorded H_β line profiles are presented in Fig. 3, which may also serve as an illustration of the experimental noise level found in their central parts.

D. Local characteristics of Stark profiles

In this paper, we focus on the central part of the H_β line profiles in order to study its asymmetry. To quantify it, sev-

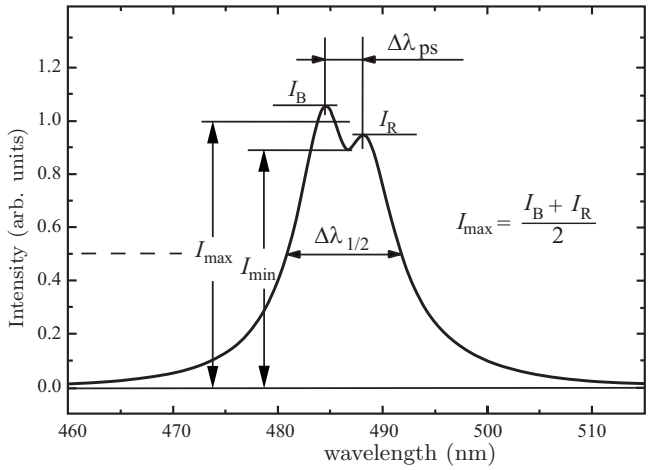

FIG. 4. Illustration of measured H_β profile parameters.

eral conventional and spectrally local characteristics of Stark profiles are used. We note that the central part of this line is easily measured, so that a good quantification of its asymmetry could be used as a reliable plasma diagnostics parameter. The general aim here is to compare the variety of experimentally inferred characteristics of Stark profiles against their calculated counterparts and further classify their dependence on plasma parameters.

The first conventional spectrally local parameter we have considered is the relative difference between the maxima of the blue and red peaks,

$$\delta I = \frac{I_B - I_R}{I_B}. \tag{1}$$

This parameter evidently describes one of the widely known asymmetry features of the H_β Stark profile, which initially inspired the interest in this phenomenon.

The second spectrally local parameter is the depth of the relative dip,

$$D_I = \frac{I_{max} - I_{min}}{I_{max}}. \tag{2}$$

In addition, the peaks separation

$$\Delta\lambda_{ps} = \lambda_R - \lambda_B, \tag{3}$$

and its ratio to the FWHM,

$$\Delta\lambda_{pshw} = \frac{\Delta\lambda_{ps}}{\Delta\lambda_{1/2}}, \tag{4}$$

are analyzed as well. The latter two parameters are primarily determined by the microfield distribution, and have received little attention by the scientific community as only small deviations are expected between the predictions of different theoretical calculations. The definitions of measured spectrally local Stark profile parameters are shown in Fig. 4.

III. STANDARD CALCULATIONS

This section is devoted to a brief description of the standard theory (ST) approach that was used for the comparison with the present experiments based on a series of papers [25,30,33,44,61].

A. Asymmetry description within ST assumptions

The ST approach considered here consists of two methods. These methods allow us to classify and consider separately the causes of asymmetry, as shown in [62]. The first ST method is based on the perturbation expansion in the line contour over the quadrupole interaction and takes into account the quadratic Stark effect [61]. It was applied earlier for the treatment of experimental data in Refs. [33,44]. Hereon, these newly generated theoretical results for the conditions of the present experiments will be denoted as "PQST" [61].

The main advantage of the second ST method is avoiding the use of perturbation theory over quadrupole interaction in the contour of spectral lines, under the simultaneous account of the quadratic Stark effect (QSE) in the ion microfield. This is achieved by using the Hamiltonian averaged over microfield nonuniformity tensor components, as first proposed in [47]. In this nonperturbative ST method (NPQST) [54,62], the following sources of asymmetry are accounted for: (i) the constrained quadrupole interaction averaged over ion microfield nonuniformity tensor components with the ion microfield strength vector being fixed; (ii) the quadratic Stark effect; (iii) the trivial asymmetry associated with conversion of cyclic frequency scale to the wavelength scale [54,62]. In the PQST, the same items are included, but in distinction from the nonperturbative approach the first item appears only after the expansion of resolvent [25].

In accordance with ST settings [21,63,64], the symmetric Stark profiles in zeroth approximation are formed by the electron impact broadening of the Stark components in the quasistatic ion microfield, taking into account the frequency shifts due to the linear Stark effect. But the ST results for asymmetric Stark profiles considered in the present work include additionally the frequency shifts due to QSE and the constrained quadrupole interaction in NPQST approach. At the same time, the corrections to the intensity of Stark components stemming from QSE and the constrained quadrupole interactions [33,44,54,61,62,65–68] are analyzed as well. The QSE corrections to intensities of Stark components are taken from [69], and in earlier publications [33,44,54,61,62,66–68] their strong influence on the asymmetry behavior was already demonstrated. In contrast to our analysis of the quadratic Stark effect, the treatment given in [31,47,48] excludes the QSE corrections to the intensity. Furthermore, the present study deals with the influence of the constrained quadrupole interaction on matrix elements of the electron impact broadening operator (see [25,30,33,44,54,61,62]).

It should be noted that resulting corrections to the contour due to various interactions are nonadditive in the NPQST approach (see [54,62]), contrary to the PQST approach used in [25,30,33,44,61]. To simplify the computations, the diagonal approximation for the electron impact broadening operator and the no-quenching approximation are used for the electron impact width evaluations [25,30,33,44,54,61,62].

This simplification is widely used in practical calculations and proven to give quite satisfactory results. In our case, we need to follow the approximate (within the first-order perturbation theory) diagonalization of resolvent due to the constrained quadrupole interaction. If the off-diagonal matrix elements of the electron broadening operator were also added, then it would appear to be a competition between the mentioned interactions. This would in turn hinder severely our ability to interpret the comparison of PQST and NPQST approaches. In the ST calculations of the total asymmetric Stark profiles, we include the electron collision shifts, evaluated within the different approach based on the kinetic Green's function technique, developed in [31,48,70].

The ST calculations of asymmetric Stark profiles are based on consideration of joint distribution functions of the electric microfield strength vector and the independent components of its tensor of nonuniformity [25]. As the formidable task of direct and detailed computations of these complex functions is not yet attempted, we approach this difficult statistical problem in terms of the first moments approximation for the microfield nonuniformity tensor components [25]. To make comparison more straightforward, we assume the Holtsmark microfield distribution function and its corresponding universal functions, describing the first constrained moment of the microfield nonuniformity tensor [25]. These functions are derived directly from the initial joint distribution function, thus making the approximate statistical solution reasonable and meaningful [25]. It is known that the Holtsmark microfield distribution function [21,63] leads to the more broad Stark profiles with smaller peak intensities in comparison with the distribution functions accounting for the weak plasma coupling (see [21]).

At the same time, the parabolic set of wave functions is chosen for the zeroth-order wave functions [25,30,33,44,54,61,62,64–68]. The latter, in conjunction with the aforementioned diagonal approximation, tends to overestimate the electron broadening in the center of the line as a direct consequence of omitting the off-diagonal matrix elements of the electron broadening operator [64] in a parabolic basis. Thus in comparison with the conventional ST results for symmetric Stark profiles [21], the described procedure overestimates the broadening due to ions and electrons within the settings of ST [21,63,64]. In particular, this causes an earlier disappearance of the red peak of H_β with the increase of electron density N_e, and leads to slight disagreement between calculated and observed [6,9,71–73] asymmetry behavior.

This is one of the reflections of the important general thesis stated earlier in [25,30,74], that the asymmetry analysis requires calculations of the total contour, contrary to what was argued and done in earlier works (for further details, see [30]). In addition, asymmetry is a sensitive multiparameter function of the broadening mechanisms, affecting the Stark profiles of hydrogen spectral lines, and is subject to the choice of the reference point [33,44,61,62].

B. Results

An analysis of the comparison of the above-described ST approach with the present experimental results is shown in Fig. 5, where the contributions to the H_β peaks asymmetry, δI, coming from various effects are indicated as well. The theoretical δI values in Fig. 5 are obtained in the course of the present work from the full H_β Stark profile calculations [54,61,62] using the PQST and NPQST approaches developed in [25,30,33,44,54,61,62]. The experimental data presented in Fig. 5 in fact correspond to the different values of plasma temperature.

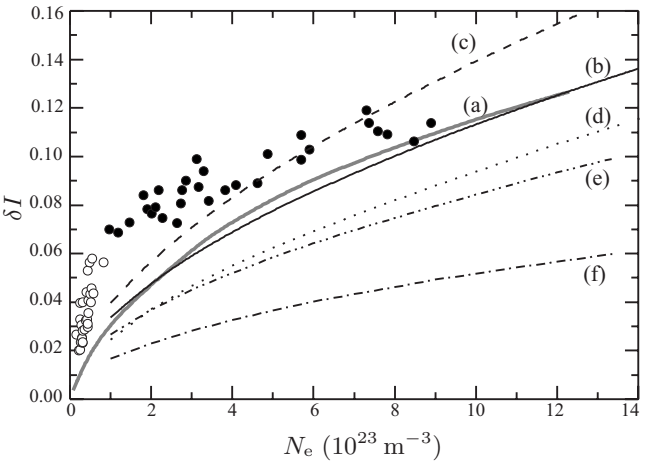

FIG. 5. Comparison of experimental Balmer-beta line peak asymmetry δI vs the electron density N_e with PQST [61] and NPQST [54] theoretical calculations: black and white circles, the collection of present experimental results; (a) the gray line, PQST calculations within perturbation approach; (b) the thin solid line, NPQST calculations without perturbation expansion with respect to the constrained quadrupole interaction; (c) the dashed line, NPQST with the electron impact widths reduced by factor 1.4; (d) the dotted line, NPQST with omitted constrained quadrupole contributions (QD); (e) the dashed-double-dotted line, NPQST with the omitted quadratic Stark effect contributions (QS) both to frequencies and intensities; (f) the dashed-dotted line, NPQST with omitted contributions due to conversion from the frequency to the wavelength scale.

The NPQST theoretical curves in Fig. 5 correspond to retaining all itemized factors at once or to excluding one of them while the rest are kept present. Such a comparison is necessary due to the nonlinear interference of each contribution in the nonperturbative framework. It is worthwhile to point out not only the better agreement with experimental results in the case of reduced impact electronic widths of Stark components, but also the drastic sensitivity of the peaks asymmetry to the electron impact widths values as was argued previously [62]. Indeed, it was noticed earlier that the quasistatic binary result of Kudrin and Sholin for the quadrupole H_β asymmetry [23] is strongly damped by the introduction of the impact electron broadening just due to the profile renormalization [25]. Thus, it could now be stated that the decrease of the impact electron broadening leads to the increase of peaks asymmetry—a reasonable interdependence not established before.

The above comparison demonstrates the importance of the correct inclusion of all significant sources of asymmetry, especially those that are inherent to experiment such as the conversion from the cyclic frequency scale to the wavelength

scale. At the same time, the reduction of electron impact widths causes the dip between peaks to become more pronounced [30,62]. This particular sensitivity of the central dip on the electron broadening was at the time a reason to misjudge the importance of ion dynamics, and led to the conclusion that the electron broadening should be described in light of a different theoretical approach than just the impact approximation [75].

Besides the diagonal approximation, there are two additional causes for deviation of the electron impact widths obtained in two different ST methods. The first one relates with the effect of incomplete collisions, which was approximately included in [76] by introducing the empirical cutoff and redefining the expression for the logarithm. It is known that the introduction of such cutoffs results in a certain decrease of impact widths. The second source is identified in more rigorous approaches that predict a decrease in electron broadening of Stark components (see [77] and reference therein) by redefining the contribution of the "strong collision" term. However, these improvements lie beyond the aim of the present ST study, as we set out initially to show how sensitive the peak asymmetry δI is on a description of the electron broadening. In that sense, it is seen from Fig. 5 that in the NPQST approach the contribution to the peak asymmetry due to the quadratic Stark effect is a bit larger than that of quadrupole interaction, but still of the same order of magnitude. In general, this behavior more or less conforms to the results of [31] but only after considering the influence of the quadratic Stark effect on oscillator strengths, which led to a reduction of the QSE's overall contribution from Ref. [31] to the peak asymmetry. The absolute partial values from [31] do not coincide with the present results, because the influence of the quadratic Stark effect on oscillator strengths has been omitted in [31], and due to the obvious difference in formalisms. On the other hand, Griem's earlier work on the subject [45] is confirmed in its general ideas, as the result of Kudrin and Sholin [23], criticizing [45], overestimated the quadrupole interaction contribution due to the neglect of the electron impact broadening. Figure 5 also demonstrates the small difference between the results of perturbative PQST and nonperturbative NPQST approaches. Moreover, the detailed study of the various asymmetry characteristics [54,61] has shown that the results of both approaches are similar to each other (see also [62]). More importantly, the nonperturbative approach allows us to avoid the diagonal approximation for the electron broadening operator and perform the calculations of the asymmetric Stark profiles via the inversion of the resolvent [21,64]. This approach, combined with the implementation of the Baranger-Mozer cluster expansion (to derive the joint distribution function for microfield and its tensor of nonuniformity; see [46,78]), would minimize the conceptual difference between the present approximate calculations and the conventional ST symmetric Stark profiles [21], and would also improve the calculated asymmetry behavior.

The electron collision shifts, generated within the Green's function approach by Sörge and Omar [48,70], were included in our ST calculations. These shifts are responsible, in particular, for the dip shift with respect to the location of the unperturbed wavelength of the H_β line [33,38,40,43,61]. Currently there is confidence only in the realistic order of magnitude of the electron collision shifts values ($\sim$1 Å for the present density range) since their theory is not fully developed [62] and their precise experimental measurements are quite troublesome [33,40,43]. Nevertheless, the present study shows that even in the case of simplified ST calculations (perturbative approach for the quadrupole interaction in the contour, Holtsmark's microfield distribution function, and diagonal approximation for impact operator), it is possible to achieve a good fit of the experimental profiles by slightly changing the electron density and temperature assigned to the particular measurements (assuming $T_e=T_i$). These values of plasma density and temperature, obtained from the above fitting procedure, often differ to some small extent from those assigned to the given Stark profile using the conventional recommendations from [21]. As Holtsmark's distribution is wider than that of Baranger-Mozer, the extracted values for density using the simplified ST approach are a bit smaller than the conventional ones. The same conclusion is reached through the implementation of the diagonal approximation in the parabolic basis.

The values and signs for electron collision shifts turned out to be important for a description of the spectrally dependent asymmetry parameter $A_1(\Delta\lambda)$ (for definition, see, for example, [44]), as demonstrated in our previous work [62]. At the same time, we were unable to establish the direct relation between asymmetry parameter $A_1(\Delta\lambda)$ and the asymmetry of peaks δI. Recall that the parameter δI is attributed to the different detunings in the red and blue parts of the profile, corresponding to the locations of blue and red peaks. It is worth mentioning that in the present analysis of sensitivity of the δI on plasma density, and within the current experimental accuracy, we found no significant influence of the electron collision shifts (compare with [31]). Electron collision shifts appear due to both the quenching and elastic collisions [28,70]. In the latter case, the shifts are caused by the residual quantum effects and velocity-averaged longitudinal momentum transfer to scattering electrons [28,70], not included in the conventional consideration of impact approximation with classical path trajectories of perturbing particles [21,63,64]. This elastic contribution was first pointed out by Boercker and Iglesias (see [28,70]).

The validity of the implementation of ST settings for the description of the H_β asymmetry was repeatedly discussed [51,55,62]. Indeed, in both experiments [4,6] and model simulations [55], the dip value in the center of this line was found to be sensitive to the ion dynamics and, in particular, to the ion temperature and the reduced mass of the radiator-perturber pair. But at the same time the experimental attempts to find noticeable signs of ion dynamics influence on the H_β FWHM for the plasma densities $\sim 10^{17}$ cm^{-3} failed [4,6]. In return, this feature allowed for widespread use of the quasistatic estimate of the H_β FWHM as a tool to diagnose the ion density in plasmas [21]. The experimental efforts to find correlations between the redshifts, derived from line asymmetry, and the ion dynamics effects for the Balmer alpha line also gave a negative answer [73]. These correlations are of fundamental significance, since the tracing of the contributions from the quadrupole interaction and the QSE could give a tool to study the characteristics of the transition

to the quasistatic limit via the asymmetry behavior in the line wings [25,46,73]. Namely, the gradual cancellation of the quadrupole contributions of ions and electrons as the quasistatic limit is approached could be used for testing the behavior of this transition [64–68]. At the same time, the quadratic Stark effect contributions would tend to double due to an addition to the ion part of the contribution from electrons, as long as the transition to the quasistatic limit would occur [62].

Within the ST approach to asymmetry, there are presently no obstacles to include consistently contributions from plasma coupling effects. It could be done within the Baranger-Mozer formalism elaborated in [46,78–81] taking account of the electron Debye screening of the ion microfields, ion-ion correlations, the quadrupole interaction, and plasma polarization effects, introduced in [79]. Presently the account of plasma coupling could be performed only within the first moments approximation for the microfield nonuniformity tensor components, since the calculations of the joint distribution function are not yet computationally feasible [25]. The corresponding universal functions of the reduced microfield strength value, β, describing the first moment of microfield nonuniformity tensor and polarization effects, are calculated and studied in [46,78] (see also [29]). Nevertheless, such work should be carried out along the lines of the present study in order to allow for consecutive analysis of various asymmetry sources [62].

It is worthwhile to note that in the context of the aforementioned plasma coupling consideration, it was found that the approach used in Ref. [38] is similar to the present PQST study of the δI parameter, the apparent difference being the use of Hooper's [1] instead of Holtsmark's [25] microfield distribution. However, the author of Ref. [38] inconsistently used the first moment for the nonuniformity tensor from [25], which is in turn based on the notion of Holtsmark distribution. On account of the more pronounced maximum of Hooper's distribution with respect to Holtsmark's, the contributions to asymmetry due to QI and QSE should only increase, thus improving the quality of fitting of the theoretical curves to the experimental data found in Fig. 5. However, any detailed study of the influence of plasma coupling effects on asymmetry would only overload this already extensive work.

Several other sources of asymmetry were not included in the presented calculations, such as the Boltzmann factors and ω^4 scaling factor for intensity [21,44], the dissolution effect in strong microfields [74], the contribution of the octupole interaction, and the second order of the constrained quadrupole interaction, which have to be included simultaneously with the quadratic Stark effect [25,30,33,44,62,65–68]. The additional inclusion of the first two factors was recently analyzed in [62], but the study of the latter and all other mentioned effects is beyond the limited scope of the present work. But even though there are other contributions of the same order, such as the second-order quadrupole corrections to the wave functions and the octupole corrections to energies, the consideration of asymmetry features restricted by only the first-order quadrupole and quadratic Stark effects has its own instructive significance [25,30,33,44,62,65–68].

The results of calculations presented in this and forthcoming sections were thoroughly checked for self-consistency against the known asymptotic dependencies and results of previous studies [25,27,28,31,33,40,62]. The present study shows that the employed physical model is able to explain the asymmetries observed experimentally without major changes in it. However, a most reliable fitting of the central part of the experimental profiles also implies proper inclusion of ion dynamics—a requirement that our present ST framework is not able to fulfill.

IV. COMPUTER SIMULATIONS

The simulation techniques have been employed previously for preparing plasma diagnosis tables [22,55,82], and for studying isolated physical effects [83–85]. However, in general, simulation studies have not taken into account the effects that give rise to the asymmetry of Balmer lines, though recently some calculation techniques [49,50,86,87] have been developed allowing to include those effects in a natural way in the simulation process. One of those recent works [87] already pointed out that these calculation techniques can give reliable results for line asymmetries and shifts. Of course, including these phenomena will improve the comparison between experiment and calculations and will give a clearer insight into the physical effects responsible of the line asymmetries. However, for the case we are dealing with here, the Balmer beta line, these improvements will not modify noticeably the diagnostics done with this line as its FWHM is quite insensitive to the line asymmetry.

A. Calculation technique

The spectral profile of a dipolar emission can be obtained as the Fourier transform of the emitter dipole moment autocorrelation function [88],

$$I(\omega) = \frac{1}{\pi}\int_0^\infty \mathrm{d}t\, \cos(\omega t)\{C(t)\}, \tag{5}$$

$$C(t) = \mathrm{tr}[\mathbf{D}(t)\cdot\mathbf{D}(0)], \tag{6}$$

$$\mathbf{D}(t) = U^+(t)\mathbf{D}(0)U(t), \tag{7}$$

with $\mathbf{D}$ being the dipole moment of the transition under study, further normalized to give $C(0)=1$, and where the time evolution operator of the system, $U(t)$, obeys the Schrödinger equation,

$$\mathrm{i}\hbar\frac{\mathrm{d}}{\mathrm{d}t}U(t) = [H_0 + q\mathbf{E}(t)\cdot\mathbf{R}]U(t). \tag{8}$$

Here H_0 is the Hamiltonian of the unperturbed emitter, $\mathbf{E}(t)$ is the electric field sequence undergone by the emitter, and $q\mathbf{R}$ is its dipole moment.

This treatment considers that two systems take part in the emission process: on the one hand, the set of emitters; on the other hand, the plasma or set of perturbers. This last one is considered as a *thermal bath* that alters the emitter evolution, but that is not affected by the emission process. In this sense, and to all intents, the plasma is always considered optically thin. Besides, the action of the plasma on the emitter has

been restricted to the electric interaction due to the charged particles in it. Optical radiation present in the plasma is not taken into account, so that the process studied corresponds to the spontaneous emission of an atom. Nearly all physical models developed to investigate Stark broadening in plasmas use these same hypotheses [14,16,18,20,21,89–93].

In addition, this work assumes that the plasma action on the emitter is limited to the dominant dipole interaction, which, naturally, is the one with the largest intensity. Neither effects due to the finite size of the emitter nor due to electric field inhomogeneities—quadrupole and higher-order effects—are going to be taken into account, because the aim of this work is to quantify only the effect of the dominant interactions. In any case, as already pointed by [49], only the quadrupole effect due to the perturber ions may be relevant. On the other hand, [49] point out that the effect may be negligible due ion dynamics.

The movement of plasma perturbers—ions and electrons—is reproduced numerically in the simulation that in turn permits us to calculate the electric microfield **E** on the emitter due to those perturbers. When the electric microfield is calculated, Eq. (8) is solved numerically to obtain the evolution of the dipole moment. In order to have a representative sampling of the microfields in the plasma, the described procedure is repeated a large number of times. Symbols $\{\}$ in expression (5) mean an average of emitters in the plasma, which in our case means an average of the emitter dipole autocorrelation functions, each of them calculated from a sequence of the perturber microfield $\mathbf{E}(t)$ obtained in the simulation.

We have considered that the plasma in our simulations is weakly coupled, homogeneous, and isotropic. Then, we assume in the simulation that the charged particles are independent and move along straight line trajectories with constant velocities that satisfy a Maxwell-Boltzmann distribution. The simulation volume considered is a sphere with the same number of ions and electrons. The emitter is static at the center of the sphere, and the relative movement between the heavy perturbers and the emitter is described using the so-called μ-ion model [83]. Due to their movement, some particles will reach the edge of the simulation sphere during the calculation. The reinjection of these particles, which is the most delicate aspect of the simulation technique, is detailed in [22] and guarantees that the statistical distributions used, homogeneity and isotropy of the particles' positions, isotropy of the paths, as well as Maxwellian distribution of velocities, are steady during the simulation [18] and that there is no correlation between the outgoing and the incoming particles.

As the perturbers considered in the simulation are independent particles, in order to take into account the correlation effects between charged particles, the electric field of the ensemble of simulated ions and electrons is evaluated at the emitter position according to the expression of the Debye shielded field [56]. The perturbers' motion as well as the emitter's evolution are carried on with the discrete *time steps* Δt. The size of these steps is chosen small enough so that the electric field $\mathbf{E}(t)$ can be considered static for the duration of each time step. In this case, the solution of the differential equation (8) is

$$U(t+\Delta t) = M(t+\Delta t,t)U(t) \simeq \exp\left[-\frac{\mathrm{i}}{\hbar}(H_0 + q\mathbf{E}(t)\cdot\mathbf{R})\Delta t\right]U(t). \quad (9)$$

For this calculation, the operator **R** includes all the transitions between all the states with principal quantum number $n=1$ to 5. Then, the main contributions to the quadratic Stark effect are included in a natural way (together with higher-order effects only for interacting levels), accounting for the main cause of the line asymmetry and shift. Consequently, quadrupolar interactions have not been taken into account at present.

To calculate the exponential (9), it is necessary to obtain the eigenvalues and the eigenvectors of the Hamiltonian. In order to ease this calculation, we have used the Cartesian basis in which all the matrix elements of the three components of **R** operator are real numbers. For the diagonalization process, we have used the Jacobi method [94]. For each time step in the simulation, one gets the numerical representation of matrix $M(t+\Delta t,t)$, see Eq. (9), which is then multiplied by $U(t)$ and promoted to the next time step.

This treatment may at first seem to be computationally very expensive. Nevertheless, modern computers permit us to carry it through without difficulties and in a reasonable time frame. Another advantage of this approach over any other numerical method for solving differential equations, such as Runge-Kutta or predictor-corrector, stems from the form of Eq. (9), which guarantees that the evolution operator is unitary during the entire simulation process. If this were not the case, nonunitarity would give rise to an artificial line broadening that would be entirely numerical in character. However, such an effect does not appear in our calculations. In order to support this statement, calculations have been repeated with decreasing values of Δt, obtaining the same converged results once the value of Δt became sufficiently small. For the value Δt considered in our simulations, the Runge-Kutta methods lead to nonunitary $U(t)$ matrices, which may give rise, in some cases, to an uncontrolled increase of the time evolution operator.

Once the evolution operator $U(t)$ is obtained, the dipole autocorrelation function must be calculated according to Eqs. (6) and (7). It is convenient to separate from the system evolution the frequencies corresponding to the energies of the unperturbed states. For this to hold, the evolution operator should be redefined as

$$U(t) \equiv \exp\left[-\frac{\mathrm{i}}{\hbar}H_0 t\right]\tilde{U}(t), \quad (10)$$

with a diagonal matrix H_0. Here, matrix $\tilde{U}(t)$ accounts for the "*modulation*" in the evolution of the emitter states due to the perturbations. In general, our interest is in plasma configurations with perturbations that give rise to "*modulations*" of very low frequency in comparison with those of the optical transitions.

Then, with this notation the autocorrelation function can be written as

$$C(t) = \mathrm{tr}\left[\tilde{U}^+(t)e^{+(\mathrm{i}/\hbar)H_0 t}\mathbf{D}e^{-(\mathrm{i}/\hbar)H_0 t}\tilde{U}(t)\cdot\mathbf{D}\right]$$
$$= \mathrm{tr}\left[e^{+(\mathrm{i}/\hbar)H_0 t}\mathbf{D}e^{-(\mathrm{i}/\hbar)H_0 t}\cdot\tilde{U}(t)\mathbf{D}\tilde{U}^+(t)\right], \quad (11)$$

making it possible to separate both domains of frequencies. The matrix $e^{+(\mathrm{i}/\hbar)H_0 t}\mathbf{D}e^{-(\mathrm{i}/\hbar)H_0 t}$ takes into account the high-frequency component of the function $C(t)$, which corresponds to the frequency of the optical transitions. This is a fixed matrix function that does not depend on the perturber field. The other matrix, $\tilde{U}(t)\mathbf{D}\tilde{U}^+(t)$, accounts for low-frequency modulations induced by the perturbations. The main motivation behind this frequency separation is the reduction of the numerical errors.

The elements of matrices $e^{+(\mathrm{i}/\hbar)H_0 t}\mathbf{D}e^{-(\mathrm{i}/\hbar)H_0 t}$ are functions of the form $D_{ij}e^{\mathrm{i}\omega_{ij}t}$. Then, one can write

$$e^{+(\mathrm{i}/\hbar)H_0 t}\mathbf{D}e^{-(\mathrm{i}/\hbar)H_0 t} \equiv \sum_k [e^{\mathrm{i}\omega_k t}\mathbf{D}_k + e^{-\mathrm{i}\omega_k t}\mathbf{D}_k^+], \quad (12)$$

where $\mathbf{D}_k$ (or $\mathbf{D}_k^+$) is the part of the matrix $\mathbf{D}$ that connects the states whose unperturbed energy separation is $\hbar\omega_k$ (or $-\hbar\omega_k$). This expansion may be translated to the autocorrelation function in the following way:

$$C(t) = \sum_k \mathrm{tr}[(e^{\mathrm{i}\omega_k t}\mathbf{D}_k + e^{-\mathrm{i}\omega_k t}\mathbf{D}_k^+)\cdot\tilde{U}(t)\mathbf{D}\tilde{U}^+(t)]$$
$$= \sum_k \cos(\omega_k t)C_k^c(t) - \sin(\omega_k t)C_k^s(t), \quad (13)$$

where

$$C_k^c(t) \equiv \mathrm{tr}[(\mathbf{D}_k + \mathbf{D}_k^+)\cdot\tilde{U}(t)\mathbf{D}\tilde{U}^+(t)], \quad (14)$$

$$C_k^s(t) \equiv \mathrm{tr}\left[\frac{1}{\mathrm{i}}(\mathbf{D}_k - \mathbf{D}_k^+)\cdot\tilde{U}(t)\mathbf{D}\tilde{U}^+(t)\right], \quad (15)$$

are both real functions. In order to calculate the line profile, the above expressions are inserted into Eq. (5),

$$I(\omega) = \sum_k \frac{1}{\pi}\int_0^\infty \mathrm{d}t\cos(\omega t)\{\cos(\omega_k t)C_k^c(t) - \sin(\omega_k t)C_k^s(t)\}. \quad (16)$$

The evaluation of the products $\cos(\omega t)\cos(\omega_k t)$ and $\cos(\omega t)\sin(\omega_k t)$ gives rise to terms in $\cos[(\omega\pm\omega_k)t]$ as well as $\sin[(\omega\pm\omega_k)t]$. Terms in $(\omega+\omega_k)$ take account of frequencies that do not appear in the correlation functions $C_k^c(t)$ and $C_k^s(t)$. These are slow varying functions in time so those products can be disregarded here. In this way,

$$I(\omega) = \sum_k \frac{1}{\pi}\int_0^\infty \mathrm{d}t(\cos[(\omega-\omega_k)t]\{C_k^c(t)\}$$
$$+ \sin[(\omega-\omega_k)t]\{C_k^s(t)\}), \quad (17)$$

which corresponds to the profiles of all the possible transitions between the studied groups of states. In our case, as already pointed out, all the states with principal quantum numbers between $n=1$ and 5 have been considered. Of course, the calculation of the Balmer-beta line only involves the term in the sum of Eq. (17) that corresponds to the transition $n=4\rightarrow 2$, but all the states mentioned above were included in the calculation of the time evolution operator $\tilde{U}(t)$. Note that Eq. (17) sets apart the symmetrical and antisymmetrical components of the profile according to the two components of the emitter dipole autocorrelation function, as defined in Eqs. (14) and (15), respectively.

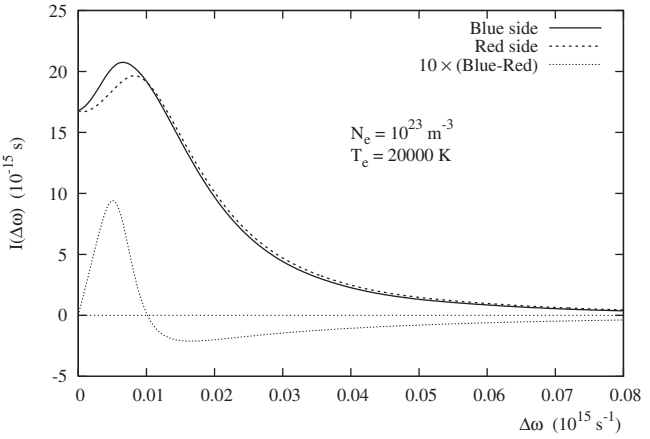

FIG. 6. Blue and red wings of a typical Balmer-beta profile obtained in the simulation and in the absence of trivial asymmetry. The antisymmetrical part of the profile, which corresponds to the sinus transformation in Eq. (17), is enlarged by factor of 10 for demonstration purposes only. The detuning of $\Delta\omega=0$ corresponds to the unperturbed line frequency.

B. Results

Figure 6 shows blue and red parts of the line profile and the antisymmetric part of a profile obtained in the simulation. This figure illustrates the profile dependence on the angular frequency detuning, without the additional asymmetry due to the change to wavelengths. An extensive convergence analysis was performed with respect to the enlargement of the number of levels used in the calculation. For this purpose, H_β profiles were generated for a variety of plasma conditions and monitoring the coupling of the levels from the first five or six atomic n-manifolds. Figure 7 shows a comparison of the profiles obtained for a pure hydrogen plasma with electron density $N_e=10^{24}$ m^{-3} and $T=10\,000$ K, taking into account in the calculation (a) all the levels between $n=1$ and 5, and (b) all the levels between $n=1$ and 6 manifolds. As can be seen, for this sufficiently high density, the differences in the line center for these two calculations fall well within the uncertainty range of the simulation. Consequently, to reduce the computational effort, all the computer simulations done here are performed using atomic levels of n-manifolds up to $n=5$. Figure 8 shows a typical outcome of comparing the recent experimental results [44] with a profile obtained in our simulations. This calculated profile includes the trivial asymmetry, and its asymmetry is clearly indicated in the different heights of H_β peaks.

V. CROSS ANALYSIS OF LOCAL STARK PROFILE CHARACTERISTICS

The data for δI parameter, see Eq. (1), obtained in the present and other experiments [9,11,13,37,38,41,42], are

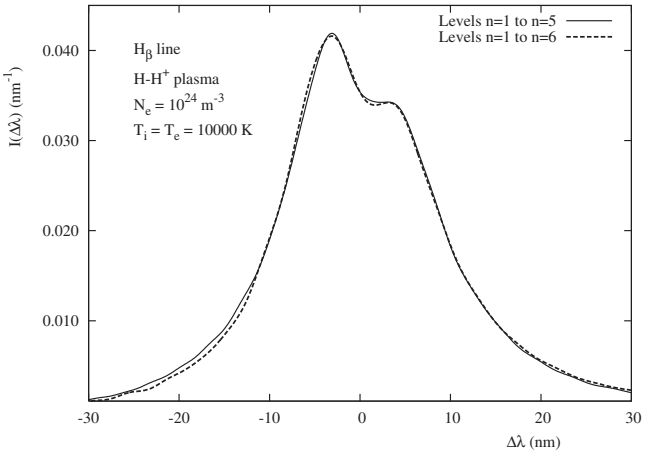

FIG. 7. Comparison of the line profiles obtained in the simulations considering coupling between the states of the first five or six atomic levels. For the conditions of the calculation, no noticeable difference can be seen beyond the intrinsic random errors of the simulations. Populations were distributed equally in all sublevels.

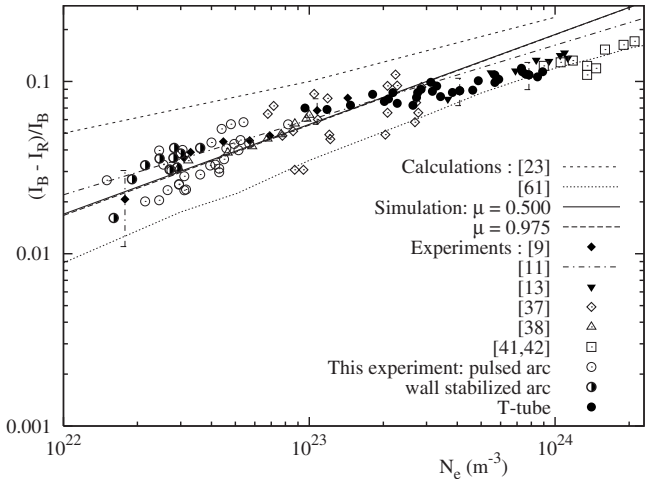

FIG. 9. Asymmetry of H_β peaks, δI, as a function of electron density, N_e. Pulsed-arc and T-tube experiments, as well as theoretical calculations, correspond to pure hydrogen plasma, while the wall-stabilized arc experiment involves an Ar-H mixture.

shown in Fig. 9 and compared with the pioneering binary quasistatic calculations [23], neglecting the electron broadening, the recent PQST [61] computations, and the latest computer simulations. The experimental uncertainties are in the range $\pm(14-19\ \%)$ for T-tube experiment and $\pm(16-20\ \%)$ for pulsed arc experiment and about $\pm 12\%$ in the wall-stabilized arc experiment. The experimental results of this work, shown in Fig. 9, correspond to a pure hydrogen plasma (T-tube and pulsed arc) and to a mixture of 98% Ar +2% H (stabilized arc). The first case corresponds to a reduced mass $\mu=0.5$ and the second one to $\mu=0.975$. All experimental results follow consistently a general trend, i.e., the values δI increase with electron density. There is an obvious disagreement between measured and calculated data

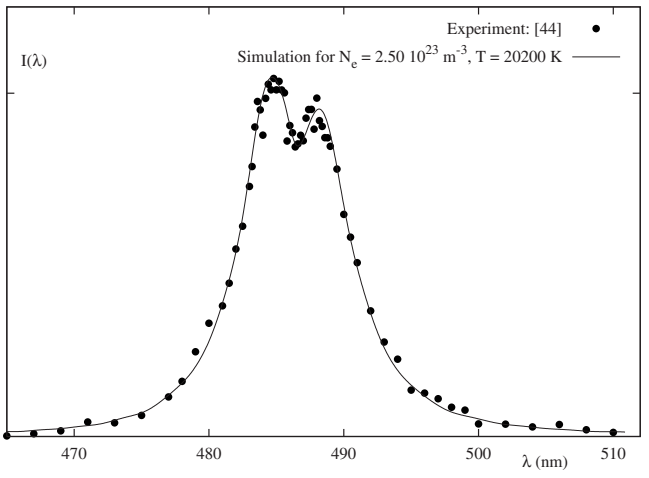

FIG. 8. Comparison of the height-normalized experimental and calculated H_β line. The experimental data correspond to the profile labeled as (2) in Fig. 6 of Ref. [44], where the authors reported an electron density of $N_e=2.73\times10^{23}$ m^{-3} and temperature $T=20\,200$ K. The simulation profile, incorporating trivial asymmetry, was generated for the same temperature but slightly lower density of $N_e=2.50\times10^{23}$ m^{-3}.

found in Ref. [23]. Theoretical curves presented by full and dotted lines in Fig. 9 are obtained in recent calculations [51,61] and in general fit well experimental data. The agreement of experimental points and PQST results [61] is a bit better for higher electron densities, while the agreement of experiment and simulations improves at lower electron densities. Both theoretical predictions for δI parameter follow the main trend of experimental points. As is well known, ion dynamics effects have an influence on the central structure of H_β line [4,6,12,15,18,61,95]. Figure 9 also shows computer simulations for the two different values of the emitter-perturber reduced mass, $\mu=0.5$ and 0.975. As is seen for these simulation results, as well as for the experimental data, a dependence of the parameter δI on ion dynamics is not observed. This is in agreement with Fig. 6 of Ref. [6], where the experimental H_β profiles for both the pure hydrogen and mixed argon-hydrogen plasma conditions are clearly compared. Although the authors of [6] analyzed the influence of ion-dynamics effects on the central dip of the line, as well as on the linewidth, they did not study the corresponding influence on the line asymmetry.

Figure 9 also illustrates a relevant result of this work. At low densities, simulations agree better with the experimental results than at high densities. This suggests that the effects considered in the simulations are enough to explain the observed asymmetries. However, at high densities the simulations give broader and more asymmetric profiles than the experimental ones. It must be taken into account that in this region the simulation technique employed in this work is in the limit of applicability. In the region of $N_e=10^{24}$ m^{-3}, the value of the coupling parameter $\rho \geqslant 0.8$ (ρ is the ratio between the mean interparticle distance and the Debye radius), which overflows the approximation of independent particles considered in these simulations. Then, more reliable results for these conditions would require us to do simulations with interacting particles, which is beyond the aim of this work. So the simulation results for high densities must be considered as an extrapolation of the model.

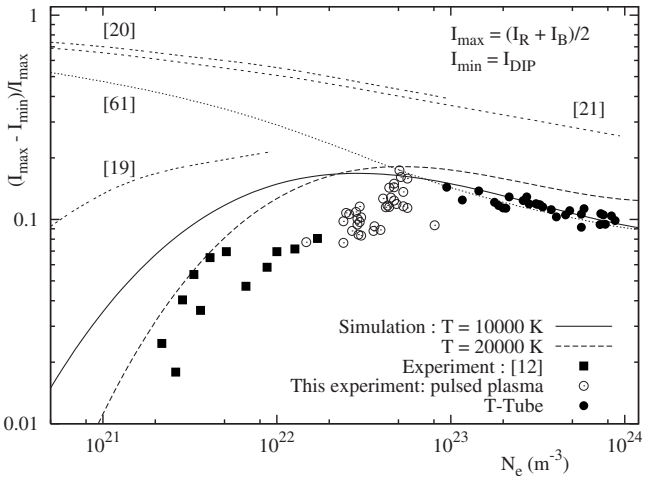

FIG. 10. Relative dip vs electron density.

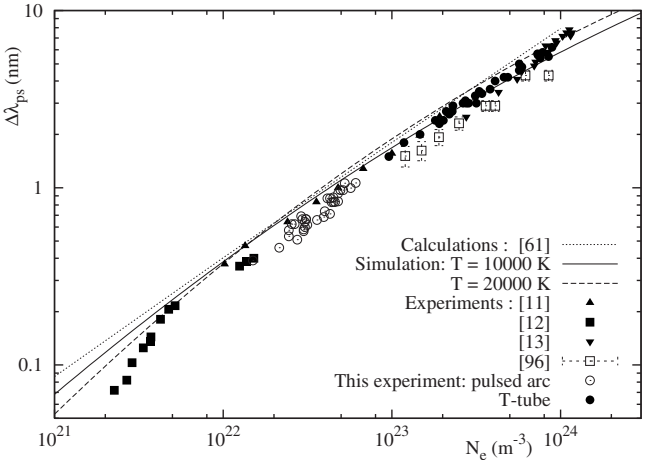

FIG. 11. Comparison of the peak separation.

For the comparison of parameter D_I, defined in Eq. (2) and shown in Fig. 10, the experimental uncertainties are in the range $\pm(19-25\ \%)$ for the T-tube experiment and $\pm(20-28\ \%)$ for the pulsed arc experiment. As can be seen in the same figure, for higher electron densities there is an agreement between experimental and theoretical relative dip results. Namely, the general functional behavior of the present experimental results is in good agreement with both computer simulations and PQST results at electron densities above 10^{23} m^{-3}. Earlier theoretical calculations [20,21] give larger relative dip values. For electron densities lower than 10^{22} m^{-3}, only the computer simulations, and in lesser capacity the model microfield method (MMM) calculations [19], are able to follow the experimental trend [12]. This is a clear indication of the influence of ion dynamics on the D_I parameter seen through the different results obtained in the simulations for different temperatures. On the other hand, in this range of plasma densities and temperatures, ions could not be considered as quasistatic, and the failure of the aforementioned ST approaches, which were never considered universal, is expected.

For the peak separation, the comparison between experimental and theoretical data is shown in Fig. 11. The experimental uncertainties are in the range $\pm(6-11\ \%)$ for T-tube experiment and $\pm(8-13\ \%)$ for pulsed arc experiment.

All theoretical data for peaks separation [19–21,44,50] are very close, especially for higher electron densities. The experimental points fit very well to the theoretical data, within the experimental uncertainties. Figure 11 suggests that the peak separation, besides the half-width, is a sensitive function of the electron density. The peak separation-to-half-width ratio can be used as a parameter for plasma homogeneity checking, as suggested in [97]. A comparison of the theoretical [19–21,61] computer simulations and experimental peak separation-to-half-width ratios is given in Fig. 12. The experimental uncertainties are in the range $\pm(8-13\ \%)$ for T-tube experiment and $\pm(10-15\ \%)$ for pulsed arc experiment. As discussed above, computer simulations and MMM calculations [19] show similar functional dependencies for lower electron densities, as they are the only calculation methods considered here that take into account ion dynamics, while the other set of analytical calculations shown in Fig. 12 considers quasistatic ions, thus giving rise to another common trend. It is important to note that the influence of ion dynamics or temperature on $\Delta\lambda_{ps}$ and $\Delta\lambda_{1/2}$ parameters is very smooth, but with slightly different dependencies, causing their ratio to exhibit the behavior shown in Fig. 12. For the conditions shown in the latter figure, dynamical effects are less important as density increases and, as a consequence, the results of all the calculations [19–21,51,61] tend to coincide. Due to the lack of experimental data for electron densities below 10^{22} m^{-3}, it is necessary to check the discrepancies found in Fig. 12. Regarding the homogeneity checks mentioned above [97], we can consider the following. In the T-tube experiment, self-absorption was less than 2% [44]. Besides the self-absorption, emission from the cold layer, formed near the tube wall, can also occur. The H_β profiles emitted from cold layers must be substantially narrower than the profiles emitted from the hot plasma. The emission from cold layers would influence the central part of the observed profile as well as the discussed conventional parameters, especially the relative dip. The thickness of the cold layer changes during the plasma lifetime, but it was much smaller than 1 mm during the plasma observation [44]. The emissivity from the cold layer is con-

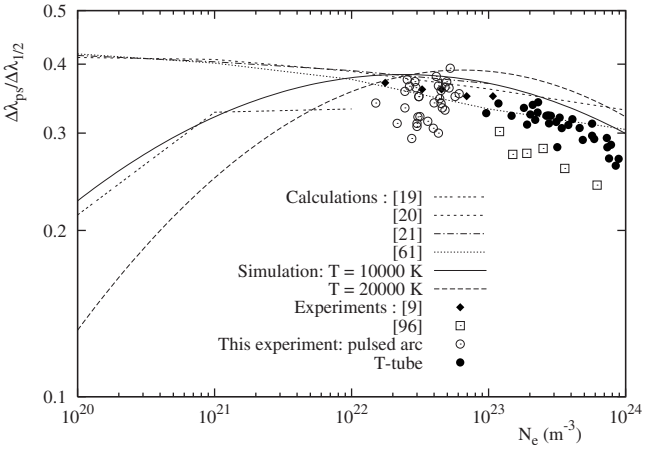

FIG. 12. Comparison of the peak separation–FWHM ratio.

sidered to be much smaller than the radiation from hot plasma mostly due to its much smaller radiation volume. Thus, for this experimental condition the influence of the cold layer could be discarded, and cannot be considered as a cause of the discrepancies between experiment and calculations. This result is also supported by a recent study on cold layers in a T-tube identical to the one employed in these measurements [98]. The thermodynamic nonequilibrium would also affect the depth of the line center, which according to Fig. 10 for T-tube experiments does not seem to be the case.

VI. CONCLUSIONS

A comprehensive study of the asymmetry of the central part of the Balmer-beta line profiles has been reported. It includes additional experimental data as well as original calculations. The comparison with other experiments [9,11–13,37,38,41,42,96] and theoretical calculations [19–21,23] has been done as well.

The use of three different plasma sources, namely electromagnetically driven T-tube, pulsed arc, and stabilized electric arc, permits one to study the line asymmetry in a wide range of plasma electron densities and temperatures. On the other hand, the two sets of ST calculations (unscreened noninteracting static ions and impact electrons with consistent account of quadrupole interaction and quadratic Stark effect) and new computer simulations (considering the coupling between all the states between $n=1$ and 5 but without quadrupole interaction) permit the estimation of the influence and validity of each approximation and considered effect via the comparison with the experimental data.

It should be emphasized that the computer simulations performed in this work allow us to account consistently for asymmetry of hydrogen Stark profiles. This means that in distinction from earlier works, the ion and electron electric field interactions with the atom are considered jointly and simultaneously on the same footing. Further study of the asymmetry phenomena of Stark profiles, with the help of the computer simulations, will offer possibilities to judge more precisely the conditions and the range of validity of the quasistatic and impact broadening regimes that are of fundamental importance for the plasma spectroscopy.

Four different conventional parameters have been analyzed in this work: the relative asymmetry of the line peaks, the relative difference between the peak average intensity and the relative dip intensity; the peak separation, and the peak separation-to-halfwidth ratio.

Though, in general, the full experimental line profiles are well reproduced by the calculations, for the low-density conditions studied here no definitive conclusion can be drawn due to a lack of experimental data. And, as can be seen in the results shown in the paper, a big disagreement between different theoretical approaches (analytical calculations and simulation results) appears in this region for some of the studied parameters. It is important to remind the reader that our experiments could not reach electron densities below 10^{22} m^{-3}, and that any new experimental results for this region will be quite revealing.

During the fitting procedure, it was found that a good fit may always be achieved by suitable temperature-density combinations. Then, any definite conclusions could be reached only on the basis of data from complementary experimental methods. Indeed, any observation of the radiation emission from gas discharges inevitably requires the complex self-consistent analysis of atomic and radiative kinetics, discharge parameters, and the character of thermodynamic equilibrium. This in turn heavily complicates the plasma diagnostics procedure and makes the interpretation of radiative spectral features quite a challenging problem [99].

The influence of ion dynamics on the line center asymmetry has been studied through the use of the well known dependence of the central dip depth on the heavy perturbers dynamics. Accordingly, the shape parameter that gives the relative distance between the peak mean intensities and the dip intensity should also depend on the ion dynamics. This has been checked by comparing different calculations with experimental results. As expected, only models that take into account ion dynamics were able to follow the observed experimental features, both in magnitude and in functional behavior. On the grounds of future efforts, it is noteworthy to reconsider the ion dynamics effects under a two-temperature plasma model [100]. Indeed, ion dynamical effects have been considered here assuming kinetic equilibrium in the plasma, as the ion temperatures were unknown in many cases. This condition is hard to fulfill for some of the experimental arrangements in this work and other experimental studies found in the literature. So, strictly speaking, in order to do a more reliable analysis of the influence of ion dynamics on the center's asymmetry, new experiments with independent measurements of electron and ion temperatures would be required.

ACKNOWLEDGMENTS

The work of S.Dj. and M.Ć. is supported by Ministry of Science and Environmental Protection, Republic of Serbia under project 141024. The work of A.V.D. has been supported by the RRC "Kurchatov institute" grants for fundamental research. The contribution of D.N. was elaborated under the support of Stockholm University. A.V.D. wishes to thank Dr. S. Sörge and Dr. B. Omar for the kind generation of the values of electron collision shifts in the $n\ell m$ quantization within Green function approach matching the experimental conditions. The work of M.A.G. and M.Á.G. has been partially financed by Spanish Ministerio de Educación y Ciencia through Grants No. ENE2004-05038/FTN and No. ENE2007-63386/FTN and by the Junta de Castilla y León through Grant No. VA032A06. The authors also want to thank the referees for their valuable suggestions and comments that helped greatly to improve the formulation of obtained results.

[1] H. R. Griem, *Principles of Plasma Spectroscopy* (Cambridge University Press, Cambridge, UK, 1997).
[2] R. A. Hill and J. B. Gerardo, Phys. Rev. **162**, 45 (1967).
[3] W. L. Wiese, D. E. Kelleher, and D. R. Paquette, Phys. Rev. A **6**, 1132 (1972).
[4] D. E. Kelleher and W. L. Wiese, Phys. Rev. Lett. **31**, 1431 (1973).
[5] D. L. Evans, D. P. Aeschilman, and R. A. Hill, Phys. Rev. A **10**, 2430 (1974); **11**, 1772(E) (1975).
[6] W. L. Wiese, D. E. Kelleher, and V. Helbig, Phys. Rev. A **11**, 1854 (1975).
[7] H. Ehrich and D. E. Kelleher, Phys. Rev. A **17**, 1686 (1978).
[8] H. Ehrich and D. E. Kelleher, Phys. Rev. A **21**, 319 (1980).
[9] V. Helbig and K. P. Nick, J. Phys. B **14**, 3573 (1981).
[10] T. L. Pittman and D. E. Kelleher, *Proceedings of the 5th International Conference on Spectral Line Shapes* (Walter de Gruyter & Co., Berlin, 1981), p. 165.
[11] J. L. Chotin, J. L. Lemaire, J. P. Marque, and F. Rostas, J. Phys. B **11**, 371 (1978).
[12] C. Fleurier, G. Coulaud, P. Ranson, and J. Chapelle, Phys. Rev. A **21**, 851 (1980).
[13] C. Carlhoff, E. Krametz, J. H. Schäfer, and J. Uhlenbusch, J. Phys. B **19**, 2629 (1986).
[14] J. Seidel, Z. Naturforsch. **32**A, 1195 (1977); **32**A, 1207 (1977).
[15] D. W. Lee, J. Phys. B **12**, 1145 (1979).
[16] R. Stamm, E. W. Smith, and B. Talin, Phys. Rev. A **30**, 2039 (1984).
[17] R. Stamm, B. Talin, E. L. Pollock, and C. A. Iglesias, Phys. Rev. A **34**, 4144 (1986).
[18] M. A. Gigosos and V. Cardeñoso, J. Phys. B **20**, 6005 (1987).
[19] C. Stehlé, Astron. Astrophys. Suppl. Ser. **104**, 509 (1994).
[20] C. R. Vidal, J. Cooper, and E. W. Smith, Astrophys. J., Suppl. Ser. **25**, 37 (1973).
[21] H. R. Griem, *Spectral Line Broadening by Plasmas* (Academic, New York, 1974).
[22] M. A. Gigosos and V. Cardeñoso, J. Phys. B **29**, 4795 (1996).
[23] L. P. Kudrin and G. V. Sholin, Sov. Phys. Dokl. **7**, 1015 (1963).
[24] G. V. Sholin, Opt. Spectrosc. **26**, 275 (1969).
[25] A. V. Demura and G. V. Sholin, J. Quant. Spectrosc. Radiat. Transf. **15**, 881 (1975).
[26] A. de Kertanguy, N. Tran Minh, and N. Feautrier, J. Phys. B **12**, 365 (1979).
[27] H. R. Griem, Phys. Rev. A **28**, 1596 (1983).
[28] D. B. Boercker and C. A. Iglesias, Phys. Rev. A **30**, 2771 (1984); H. R. Griem, *ibid.* **38**, 2943 (1988); H. R. Griem, C. A. Iglesias, and D. B. Boercker, *ibid.* **44**, 5318 (1991).
[29] J. Halenka, Z. Phys. D: At., Mol. Clusters **16**, 1 (1990).
[30] A. V. Demura, V. V. Pleshakov, and G. V. Sholin, *Atlas of Detailed Stark Profiles in Dense Plasmas* (I. V. Kurchatov Institute of Atomic Energy, Moscow, 1991), pp. 1–97 (in Russian).
[31] S. Günter and A. Könies, Phys. Rev. E **55**, 907 (1997).
[32] H. R. Griem, Contrib. Plasma Phys. **41**, 223 (2001).
[33] A. Demura, V. Helbig, and D. Nikolić, *Spectral Line Shapes*, edited by C. A. Back, AIP Conf. Proc. No. 645 (AIP, New York, 2002), Vol. 12, pp. 318–324.
[34] W. L. Wiese and D. E. Kelleher, Astrophys. J. **166**, L59 (1971).
[35] F. Torres, M. A. Gigosos, and S. Mar, J. Quant. Spectrosc. Radiat. Transf. **31**, 265 (1984).
[36] J. Halenka and J. Musielok, J. Quant. Spectrosc. Radiat. Transf. **36**, 233 (1986).
[37] Z. Mijatović, M. Pavlov, and S. Djurović, J. Quant. Spectrosc. Radiat. Transf. **38**, 209 (1987).
[38] J. Halenka, J. Quant. Spectrosc. Radiat. Transf. **39**, 347 (1988).
[39] S. Djurović, Z. Mijatović, and R. Kobilarov, Contrib. Plasma Phys. **28**, 229 (1988).
[40] J. Halenka, B. Vujičić, and S. Djurović, J. Quant. Spectrosc. Radiat. Transf. **42**, 571 (1989).
[41] J. Uhlenbusch and W. Viöl, Contrib. Plasma Phys. **29**, 459 (1989).
[42] J. Uhlenbusch and W. Viöl, J. Quant. Spectrosc. Radiat. Transf. **44**, 47 (1990).
[43] Z. Mijatović, M. Pavlov, and S. Djurović, Phys. Rev. A **43**, 6095 (1991).
[44] S. Djurović, D. Nikolić, I. Savić, S. Sörge, and A. V. Demura, Phys. Rev. E **71**, 036407 (2005).
[45] H. R. Griem, Z. Phys. **137**, 280 (1954).
[46] A. V. Demura and C. Stehlé, *Spectral Line Shapes*, edited by D. May, J. Drummond, and E. Oks, AIP Conf. Proc. No. 328 (AIP, New York, 1995), Vol. 8, pp. 177–208.
[47] R. F. Joyce, L. A. Woltz, and C. F. Hooper, Phys. Rev. A **35**, 2228 (1987).
[48] A. Könies and S. Günter, J. Quant. Spectrosc. Radiat. Transf. **52**, 825 (1994); S. Sörge and B. Omar (private communication).
[49] S. Sorge and S. Günter, Eur. Phys. J. D **12**, 369 (2000).
[50] M. A. Gigosos, M. A. González, B. Talin, and A. Calisti, *Spectral Line Shapes*, edited by E. Dalimier (Frontier Group, Paris, 2004), p. 451.
[51] M. A. Gigosos and M. Á. González, *The Physics of Ionized Gases: 23rd Summer School and International Symposium*, edited by L. Hadžievski, B. P. Marinković, and N. S. Simonović, AIP Conf. Proc. No. 876 (AIP, New York, 2006), p. 294.
[52] J. Halenka and W. Olchawa, Eur. Phys. J. D **42**, 425 (2007).
[53] R. Žikić, M. A. Gigosos, M. Ivković, M. Á. González, and N. Konjević, Spectrochim. Acta, Part B **57**, 987 (2002).
[54] A. V. Demura and G. V. Demchenko, Stark Profile Calculation Code v.2 C++ (2007): http://www.hepti.kiae.ru/~demura/SPCCv2_cpp.
[55] M. A. Gigosos, M. Á. González, and V. Cardeñoso, Spectrochim. Acta, Part B **58**, 1489 (2003).
[56] E. Dufour, A. Calisti, B. Talin, M. A. Gigosos, M. Á. González, T. del Río Gaztelurrutia, and J. W. Dufty, Phys. Rev. E **71**, 066409 (2005).
[57] S. Djurović, Z. Mijatović, R. Kobilarov, and N. Konjević, J. Quant. Spectrosc. Radiat. Transf. **57**, 695 (1997).
[58] S. Djurović, D. Nikolić, Z. Mijatović, R. Kobilarov, and N. Konjević, Plasma Sources Sci. Technol. **11**, A95 (2002).
[59] H. R. Griem, *Plasma Spectroscopy* (McGraw-Hill, New York, 1964).
[60] C. H. Popenoe and J. B. Shumaker, Jr., J. Res. Natl. Bur. Stand., Sect. A **69**, 495 (1965).
[61] A. V. Demura and D. Nikolić, Hb.nb—program for H_β asymmetry investigation (2001): http://tesla.physics.wmich.edu/dn/programs.html.
[62] A. V. Demura, G. V. Demchenko, and D. Nikolić, *On Theory*

of Hydrogen Spectral Lines Asymmetry in Plasmas (RRC "Kurchatov Institute," Moscow, 2006), pp. 1–37 (in Russian); Eur. Phys. J. D **46**, 111 (2008).
[63] I. I. Sobelman, *Introduction to the Theory of Atomic Spectra* (Pergamon, Oxford, 1972).
[64] G. V. Sholin, A. V. Demura, and V. S. Lisitsa, Zh. Eksp. Teor. Fiz. **64**, 2097 (1973) [Sov. Phys. JETP **37**, 1057 (1973)].
[65] G. V. Sholin, *On Origin of Profile Asymmetry of Hydrogen Spectral Lines in Dense Plasma* (I. V. Kurchatov Institute of Atomic Energy, Moscow, 1967), pp. 1–28 (in Russian).
[66] E. Oks and G. V. Sholin, Opt. Spektrosk. **33**, 401 (1972) [Opt. Spectrosc. **33**, 217 (1972)].
[67] M. E. Bacon, J. Quant. Spectrosc. Radiat. Transf. **13**, 1161 (1973).
[68] M. E. Bacon, J. Quant. Spectrosc. Radiat. Transf. **17**, 501 (1977).
[69] N. Hoe, E. Banerjea, H. W. Drawin, and L. Herman, J. Quant. Spectrosc. Radiat. Transf. **5**, 835 (1965).
[70] L. Hitzschke, G. Röpke, T. Seifert, and R. Zimmermann, J. Phys. B **19**, 2443 (1986); L. Hitzschke and G. Röpke, Phys. Rev. A **37**, 4991 (1988).
[71] W. L. Wiese, D. R. Paquette, and J. E. Solarski, Phys. Rev. **129**, 1225 (1963).
[72] R. C. Preston, J. Phys. B **10**, 523 (1977).
[73] D. E. Kelleher, N. Konjević, and W. L. Wiese, Phys. Rev. A **20**, 1195 (1979).
[74] B. d'Etat, J. Grumberg, E. Leboucher, H. Nguyen, and A. Poquerusse, J. Phys. B **20**, 1733 (1987).
[75] G. Peach, Adv. Phys. **30**, 367 (1981).
[76] P. Kepple and H. R. Griem, Phys. Rev. **173**, 317 (1968).
[77] S. Alexiou and A. Poquérusse, Phys. Rev. E **72**, 046404 (2005).
[78] A. V. Demura, D. Gilles, and C. Stehlé, J. Quant. Spectrosc. Radiat. Transf. **54**, 123 (1995).
[79] A. V. Demura, *Theory of Joint Distribution Functions of Microfield and Its Spatial and Time Derivatives in Plasmas with Complex Ionization Composition* (I. V. Kurchatov Institute of Atomic Energy, Moscow, 1988), pp. 1–17 (in Russian).
[80] A. V. Demura, Zh. Eksp. Teor. Fiz. **110**, 114 (1996) [JETP **83**, 60 (1996)].
[81] C. Stehlé, D. Gilles, and A. V. Demura, Eur. Phys. J. D **12**, 355 (2000).
[82] M. Á. González and M. A. Gigosos, Astron. Astrophys. Suppl. Ser. **145**, 491 (2000).
[83] J. Seidel and R. Stamm, J. Quant. Spectrosc. Radiat. Transf. **27**, 499 (1982).
[84] M. A. Gigosos, V. Cardeñoso, and F. Torres, J. Phys. B **19**, 3027 (1986).
[85] D. H. Oza, R. L. Greene, and D. E. Kelleher, Phys. Rev. A **38**, 2544 (1988).
[86] M. A. Gigosos, M. Á. González, and N. Konjević, Eur. Phys. J. D **40**, 57 (2006).
[87] E. Stambulchik and Y. Maron, J. Quant. Spectrosc. Radiat. Transf. **99**, 730 (2006).
[88] P. W. Anderson, Phys. Rev. **76**, 647 (1949).
[89] M. Baranger, Phys. Rev. **111**, 481 (1958); **111**, 494 (1958); **112**, 855 (1958).
[90] R. Stamm and D. Voslamber, J. Quant. Spectrosc. Radiat. Transf. **22**, 599 (1979).
[91] G. C. Hegerfeldt and V. Kesting, Phys. Rev. A **37**, 1488 (1988).
[92] B. Talin, A. Calisti, L. Godbert, R. Stamm, R. W. Lee, and L. Klein, Phys. Rev. A **51**, 1918 (1995).
[93] J. Halenka and W. Olchawa, J. Quant. Spectrosc. Radiat. Transf. **56**, 17 (1996).
[94] W. W. Press, S. A. Teukolsky, W. T. Vetterling., and B. P. Flannery, *Numerical Recipes in C* (Cambridge University Press, New York, 1997).
[95] V. Cardeñoso and M. A. Gigosos, Phys. Rev. A **39**, 5258 (1989).
[96] C. Parigger, D. H. Plemmons, and E. Oks, Appl. Opt. **42**, 5992 (2003).
[97] W. L. Wiese, in *Physics of Ionized Gases*, edited by V. Vujnović (Rovinj, Yugoslavia, 1974), pp. 637–673.
[98] M. Pavlov, S. Djurović, B. Vujičić, R. Kobilarov, and Z. Mijatović, Plasma Sources Sci. Technol. **18**, 015018 (2009).
[99] S. Adamson, V. Astapenko, I. Chernysheva, V. Chorkov, M. Deminsky, G. Demchenko, A. Demura, A. Demyanov, N. Dyatko, A. Eletzkii, A. Knizhnik, I. Kochetov, A. Napartovich, E. Rykova, L. Sukhanov, S. Umanskii, A. Vetchinkin, A. Zaitsevskii, and B. Potapkin, J. Phys. D **40**, 3857 (2007).
[100] M. Á. González and M. A. Gigosos, Plasma Sources Sci. Technol. (to be published).